

Effects of Ilmenite Ore on Phase Development of Hematite Ore Sinter



EDSON KUGARA CHIWANDIKA and SUNG-MO JUNG

The effects of adding 5 to 25 wt pct of ilmenite ore to hematite ore sinter were investigated employing a horizontal tube furnace to clarify the phase development. The temperature was raised nonisothermally at 10 °C/min to 1150 °C in an Ar atmosphere. When the target temperature was reached, 1 L/min of air was injected to allow combustion of the carbon in the pellets. The development of the phases in the sinters was studied using X-ray diffraction (XRD), energy-dispersive X-ray spectroscopy (EDS), and electron probe microanalysis (EPMA). The tumbler index (TI) decreased with the increase in ilmenite addition up to 20 wt pct, which increases TiO₂ (s) and Fe₃O₄ (s) content in the sinter blends. Addition of more than 2 wt pct TiO₂ (s) to the sinter blends resulted in the formation of perovskite (CaO·TiO₂), which affected the development of bonding phases. These changes deteriorated the reduction degradation index (RDI). The estimated melt formation temperature of the sinter blends increased with ilmenite addition up to 15 wt pct and decreased thereafter. An attempt was made to predict the development of phases in the ternary phase diagram of CaO-Fe₂O₃-TiO₂. The reduction behavior of the sinter blends was affected by the type of the bonding phase.

<https://doi.org/10.1007/s11663-020-01856-2>

© The Minerals, Metals & Materials Society and ASM International 2020

I. INTRODUCTION

Titanium-containing ores are one of the underutilized abundant resources in the world. Uses of these ores are limited due to the lack of basic sintering data, high bulk Fe₃O₄ (s) content, and presence of TiO₂ (s), which affects the development of the sinter bonding phase by forming phases such as perovskite, CaO·TiO₂ (s).^[1,2] Most of the Ti-containing ores are of poor grade and have fine mineral crystal size with numerous mineral components, which develop complicated phases during sintering.^[1]

An increase in Ti in the sinter mix may negatively affect the reduction degradation index (RDI),^[1-7] but this effect is not clear. CaO·TiO₂ (s) distributed in the glass phase can decrease its mechanical strength and facilitate crack propagation.^[1]

TiO₂ (s) in titanomagnetite ore was reported to react with CaO in the molten silico-ferrite of calcium aluminum (SFCA) at high temperature; this process led to the precipitation of the Fe₂O₃ (s), 2CaO·SiO (s), and CaO·TiO₂ (s) out of the SFCA.^[2] Accordingly, the RDI deteriorated because of volume expansion from the reduction of Fe₂O₃ (s) to Fe₃O₄ (s). However, in

chromium-bearing vanadium titanium magnetite with TiO₂ (s) content of 6 to 12 wt pct, CaO·TiO₂ (s) formed in the sinter but was uniformly distributed within the silicate phases and had little or no effect on the strength of the bonding phase^[8]; the RDI was improved due to formation of magnesium ferrite, which suppressed hematite reduction. However, the reducibility index (RI) of their sinter was decreased by the formation of CaO·TiO₂ (s) and 2MgO·TiO₂ (s).^[8]

Doping with up to 2 wt pct TiO₂ (s) in high-grade hematite ore can improve the sintering process by reducing the melting point of the sinter.^[4] As TiO₂ (s) content increases, the required sintering temperatures increase^[9]; Webster *et al.*^[9] used about 2.4 to 11.6 wt pct ironsand in their experiment. Ironsand usually contains ~ 8 wt pct TiO₂ (s), so the TiO₂ (s) addition was 0.2 to 1 wt pct^[3,9]; therefore, the results of Manshadi *et al.*^[4] contradict those of Webster *et al.*^[9]

Sintering aims to produce sinter containing more calcium ferrite of high strength and reducibility.^[9,10] Calcium ferrite forms two main phases, called SFCA-I and SFCA. SFCA-I has low Si and high Fe content with some platy or acicular morphology, which is responsible for the formation of some intersecting microplates. In contrast, SFCA has low Fe content and high Si content and forms prismatic or columnar morphology. SFCA is usually associated with the glass phase and, therefore, has low strength and low reducibility of sinter compared with the sinter with SFCA-I.^[9,10] The thermal stability range of SFCA lies in between 1240 °C and 1390 °C,

EDSON KUGARA CHIWANDIKA and SUNG-MO JUNG are with the Graduate Institute of Ferrous Technology, Pohang University of Science and Technology, Pohang, 790-784, South Korea. Contact email: smjung@postech.ac.kr

Manuscript submitted November 24, 2019.

Article published online June 4, 2020.

whereas that of SFCA-I has not yet been determined.^[9,10] SFCA-I and SFCA have different crystallographic structures.^[9,10] The CaO-Fe₂O₃-Al₂O₃ phase diagram also shows that compounds intermediate between SFCA-I and SFCA can form; these are called SFCA-II, about which no information is available. Specifically, the sintering mechanism during solidification should be clarified by investigating how oxide impurities affect the stability of SFCA and SFCA-I.

Effective utilization of Ti-bearing resources requires understanding of the effect of their addition, especially on hematite ore sinter, because most Ti-bearing ores have complicated mineral composition, so their sintering behaviors differ.^[4] Knowledge of the sintering behavior would allow estimation of coke content, sinter quality, and productivity. The goal of this study is to investigate how the addition of 5 to 25 wt pct of ilmenite ore affects the development of phases in hematite ore sinter, to provide basic sintering data of the hematite-ilmenite ore blends.

II. EXPERIMENTAL

A. Materials Preparation

The hematite ore was composed primarily of iron oxide and traces of oxides of Ca, Mg, Al, Ti, Cr, and V; the ilmenite ore was composed primarily of iron oxides with substantial proportions of those oxides, especially TiO₂ (Table I). The phases (Figure 1) in the initial ores before blending were identified by X-ray diffraction (XRD) using Bruker AXS (Billerica, MA) with a Cu tube with a scan angle of 20 to 80 deg at a rate of 2 deg/min, sampling 0.02 deg at a voltage of 40 kV, and current of 40 mA. The particle sizes of both ores were < 250 μm to enable easy and uniform mixing. However, in the industrial sintering process, bigger particle sizes and a different mixing procedure are used.

The basicity (CaO/SiO₂) of the hematite ore weighing 200 g was adjusted to be 2, and then 5 wt pct of pure carbon was added to the sinter mix; it was then blended for 30 minutes using a Turbula Mixer (T₂F No. 120942, Switzerland) at 34 rpm. After blending, the sinter mix was mixed with distilled water, pelletized into a spherical pellet weighing ~1.5 g, and then dried in an oven at 100 °C for 2 hours.

Approximately 5 to 25 wt pct of ilmenite ore was added to 200 g of hematite. The basicity of the blends was adjusted to be 2 using CaO (s) and 5 wt pct of pure carbon was added. The blending ratio was as shown in Table II, giving sinter blends with chemical composition shown in Tables III and IV. The hematite-ilmenite sinter

blends were uniformly mixed, pelletized, and dried according to the identical procedure used in preparing the hematite sinter blend.

B. Experimental Procedure

1. Sintering

About 50 pellets of each sinter blend were placed in a cylindrical Al₂O₃ crucible (50-mm OD × 120-mm height) and then sintered in the horizontal tube furnace (Figure 2(a)).

The temperature was raised nonisothermally at 10 °C/min to 1150 °C in Ar atmosphere. When the target temperature of 1150 °C was reached, 1 L/min air was introduced to allow combustion of the carbon in the pellets; this combustion ensured that the samples were exposed to a range of different partial oxygen pressures and temperatures within the pellet. This procedure was intended to emulate industrial iron ore sintering, in which the raw materials are heated in low oxygen partial pressure and cooled at high oxygen partial pressure, so the exact gaseous atmosphere in real sinter is not

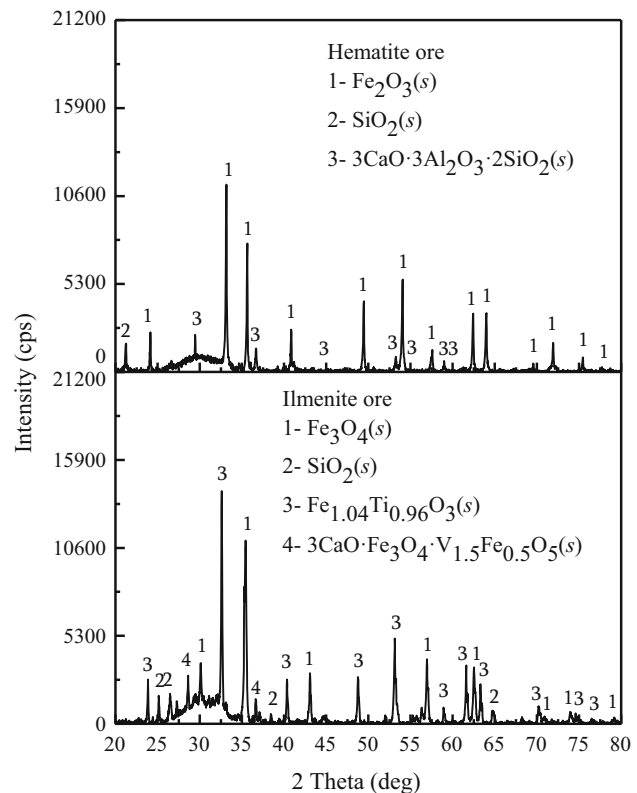


Fig. 1—XRD patterns of the hematite ore and the ilmenite ore.

Table I. Chemical Composition of the Hematite Ore, Ilmenite Ore, and CaO Used (Weight Percent)

Name of Specimen	TFe	FeO	CaO	MgO	Al ₂ O ₃	SiO ₂	TiO ₂	Cr ₂ O ₃	V ₂ O ₅	P	S
Hematite ore	62.8	0.54	0.102	0.091	1.49	1.70	0.219	0.017	0.008	0.078	0.0164
Ilmenite ore	43.4	23.0	1.44	4.48	5.29	5.39	18.9	0.050	0.518	0.074	0.308
CaO			93.8	0.584	0.081	0.931					

Table II. Blending Ratios of the Sinter Blends Used in This Study

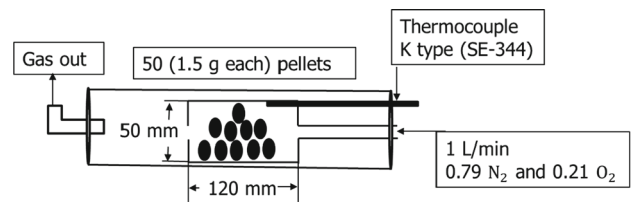
Blend	Basicity	Weight Percent			
		Hematite Ore	Ilmenite Ore	CaO	Carbon
1	2	92.00	0	3.23	4.76
2	2	87.36	4.37	3.51	4.76
3	2	83.17	8.32	3.75	4.76
4	2	79.36	11.90	3.97	4.76
5	2	75.88	15.18	4.18	4.76
6	2	72.70	18.18	4.36	4.76

Table III. Chemical Composition of the Sinter Blends

Blend	Weight Percent								
	TFe	FeO	Fe ₂ O ₃	SiO ₂	Al ₂ O ₃	CaO	MgO	TiO ₂	CaO/SiO ₂
1	57.8	0.50	82.08	1.594	1.373	3.128	0.103	0.201	1.96
2	56.8	1.48	79.56	1.753	1.535	3.442	0.296	1.017	1.96
3	55.8	2.36	77.16	1.897	1.682	3.723	0.470	1.754	1.96
4	55.0	3.17	75.11	2.027	1.815	3.978	0.629	2.424	1.96
5	54.2	3.90	73.17	2.147	1.937	4.214	0.773	3.035	1.96
6	53.5	4.57	71.41	2.256	2.048	4.427	0.906	3.594	1.96

Table IV. MgO Content in the Sinter Blend with Increasing Ilmenite Addition (Weight Percent)

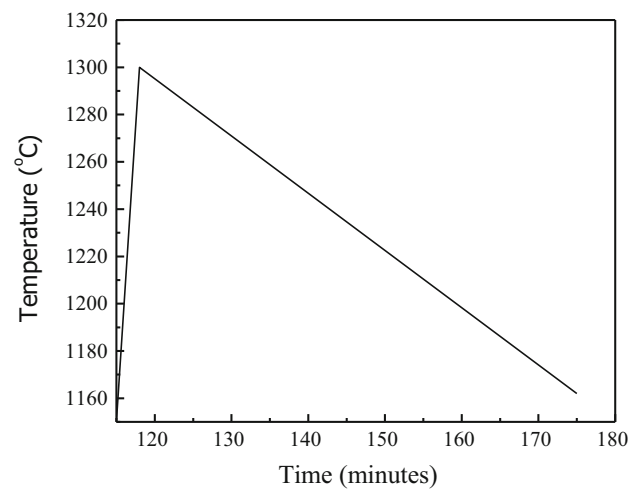
Blend	1	2	3	4	5	6
MgO (Wt Pct)	0.103	0.296	0.470	0.629	0.773	0.906



(a)

known.^[11] During an actual sintering process, heating rates are much higher than 10 °C/min; the low preheating rate in this investigation was chosen to minimize the temperature gradient within the pellet. When the target temperature of 1150 °C had been reached, the temperature was assumed to be nearly uniform throughout each sample because of the low heating rate. This uniformity was expected to maximize the number of phases formed and facilitate their identification after sintering. Phases detected were compared with those reported in the literature.^[12] The temperature during sintering was measured using a K-type thermocouple (SE-344) inserted into the sample holder shown (Figure 2(a)). The maximum temperature during sintering was about 1300 °C.

The heating profiles during sintering of blends differed negligibly. All sinter blends took about 3 minutes to reach the maximum temperature of ~ 1300 °C, and the final temperature after holding for 1 hour was between 1160 °C and 1165 °C (Figure 2(b)). The 1-hour holding time was used to allow maximum combustion of carbon. This



(b)

Fig. 2—(a) Schematic diagram of the sintering apparatus employed in this experiment. (b) Representative temperature profile after opening air.

holding time was much longer than that used in an actual sintering process and was chosen to maximize formation of bonding phases to enable easy identification of phases.

The sintered pellets were allowed to cool passively to room temperature in air. After cooling, a representative sample of each sinter was taken and prepared for electron probe microanalysis (EPMA, JEOL* JXA-8530F), energy-dispersive X-ray spectroscopy (EDS, (JEOL

*JEOL is a trademark of Japan Electron Optics Ltd., Tokyo.

JSM-7100F), and XRD (Bruker AXS) analyses. Before EDS and EPMA analyses, the sintered pellets were mounted in epoxy resin and polished. Element mapping by EPMA and point chemical by EDS analyses were done at 20 KeV using a beam current of 50 nA.

2. Tumbler Index and RDI

The sample size was small, and the modified abrasion method reported by Manshadi *et al.*^[4] was adopted to get valuable information on the tumbler index (TI) and RDI. Approximately 20 sintered pellets of known weight were prepared for the determination of TI using the modified abrasion tester.^[4] The sintered pellets were tumbled for 8 minutes at 25 rpm; TI was recorded using the weight of samples that remained above +2 mm in diameter as

$$TI_{+2\text{mm}} = \frac{\text{Weight of +2 mm fraction in mg}}{\text{Initial sample weight in mg}} \times 100 \quad [1]$$

$TI_{+2\text{ mm}}$ of 80 pct in this test is equivalent to ISO TI = 62 pct greater than 6.2 mm in the standard pot-grate sinter.^[4]

The RDI is the measure of the ability of the sinter to disintegrate in the upper part of the blast furnace. The RDI was measured by placing 10 sintered pellets of known weight into the special sample holder (Figure 2(a)) and then raising the temperature at 10 °C/min to 500 °C in an Ar atmosphere in a horizontal furnace. Then, a gas mixture consisting of 60 vol pct Ar, 20 vol pct CO, and 20 vol pct CO₂ was injected for 1 hour. The resulting partially reduced pellets were cooled to room temperature in Ar atmosphere and then tumbled at 30 rpm for 10 minutes using the same apparatus used to determine $TI_{+2\text{ mm}}$. The $RDI_{+2\text{ mm}}$ was evaluated as the weight of samples that retained a diameter >2 mm as

$$RDI_{+2\text{mm}} = \frac{\text{Weight of +2mm fraction in mg}}{\text{Initial sample weight in mg}} \times 100 \quad [2]$$

3. Melt formation temperature

The melt formation temperature of each sinter blend was estimated using the thermogravimeter–differential scanning calorimeter (TG-DSC) (TGA/DSC 1 Star system, Mettler Toledo). A powder sample of each sinter blend weighing about 100 mg was placed into an Al₂O₃ crucible (7-mm ID × 8-mm OD × 4.5-mm height) and placed into the TG-DSC furnace. The temperature was raised

nonisothermally at 20 °C/min in an Ar atmosphere from room temperature to 1300 °C. The melting temperature was estimated using the heat flow in terms of the DSC.

4. Reduction behavior of the sintered blends

Reducibility is the measure of how easily the oxygen combined with iron can be removed indirectly.^[13] The percentage reduction degree was evaluated as follows:

$$\text{Degree of reduction(pct)} = \frac{n_0 - n}{n_0} \times 100 \quad [3]$$

where n_0 is the number of moles of oxygen in the original sample before reduction and n is the number of moles of oxygen left in the reduced sample. The value of n_0 for each sinter in this investigation was evaluated by summing the amount of oxygen attached to Fe and the amount of oxygen attached to Ti. The amount of oxygen removed from the sample was measured by thermogravimetric analysis (TGA).

The changes in reduction degree in this experiment were measured at an isothermal temperature of 1000 °C in a gas mixture of 60 vol pct Ar and 40 vol pct CO at 1 L/min for 4 hours using TGA (Rubotherm KOR 808). For the sake of comparison, the RI, dRD/dt (O/Fe = 0.9), values at 40 pct reduction degree of each sinter were evaluated using the following equation^[14]:

$$RI = \frac{dRD}{dt} \left(\frac{O}{Fe} = 0.9 \right) = \frac{33.6}{t_{60} - t_{30}} \quad [4]$$

where t_{30} and t_{60} are the time required to attain the reduction degree of 30 and 60 pct (minutes), respectively.

III. RESULTS AND DISCUSSION

A. TI and RDI with Increasing Ilmenite Addition

$TI_{+2\text{ mm}}$ and $RDI_{+2\text{ mm}}$ were both affected by ilmenite addition (Figure 3). $TI_{+2\text{ mm}}$ remained approximately unchanged up to 10 wt pct ilmenite addition, decreased to a minimum at 20 wt pct ilmenite, and then

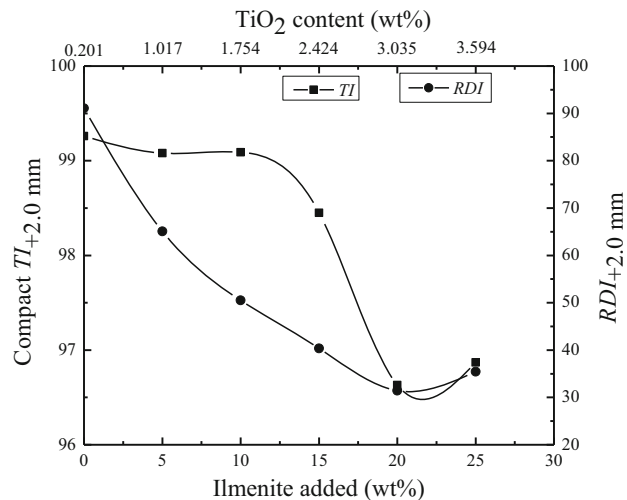


Fig. 3—TI and RDI (s) with increasing ilmenite addition.

increased as the ilmenite percentage was increased further. Generation of fines measured by $RDI_{+2\text{ mm}}$ increased with an increase in ilmenite addition up to 20 wt pct, and thereafter began to decrease. Ilmenite contains Fe_3O_4 (s) as well as TiO_2 (s) and other gangue material, so the phase change in the sinter might be related to the change in $TI_{+2\text{ mm}}$ and $RDI_{+2\text{ mm}}$. The changes in phase were investigated using XRD, EDS, and EPMA analyses.

B. Phase Development with Increasing Ilmenite Addition

A representative sample of each sinter blend was crushed and taken for XRD analyses to investigate the phases formed after sintering with increasing ilmenite addition (Figures 4(a) through (f)). The main bonding material in sinter made from blend 1 consisted of some derivatives of calcium ferrite (Figure 4(a)). The bonding phases in sintered blend 1 were $\text{Ca}_{3.18}\text{Fe}_{15.48}\text{Al}_{1.34}\text{O}_{28}$ (s)

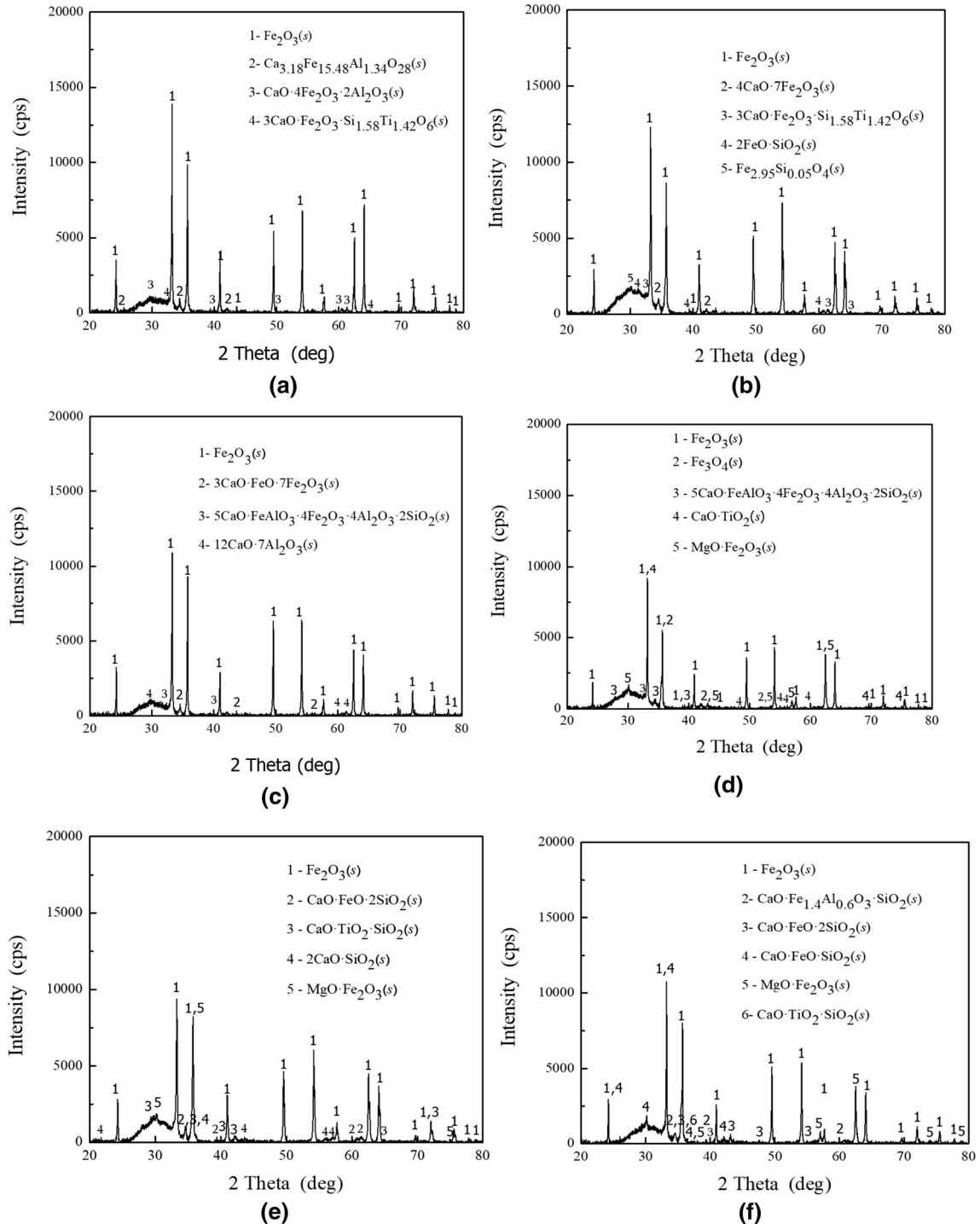


Fig. 4—XRD analyses of (a) sintered blend 1, (b) sintered blend 2, (c) sintered blend 3, (d) sintered blend 4, (e) sintered blend 5, and (f) sintered blend 6.

(ICDD 01-089-0599), $\text{CaO}\cdot 4\text{Fe}_2\text{O}_3\cdot 2\text{Al}_2\text{O}_3$ (s) (ICDD 00-049-1586), and $3\text{CaO}\cdot \text{Fe}_2\text{O}_3\cdot \text{Si}_{1.58}\text{Ti}_{1.42}\text{O}_6$ (s) (ICDD 01-078-0319). Calcium ferrites are the most important intermediate compound for formation of SFCA, which is the most important bonding phase in sinter.^[10] Assimilation of the aluminum and silicon into the calcium ferrite formed the calcium ferrite aluminates and silicates. The general formula of SFCA-I has been reported^[12] to be $\text{M}_{20}\text{O}_{28}$, of SFCA as $\text{M}_{14}\text{O}_{20}$, and of SFCA-II as $\text{M}_{34}\text{O}_{48}$, where $\text{M} = \text{Fe}, \text{Ca}, \text{Si}, \text{and Al}$. The current results identified $\text{Ca}_{3.18}\text{Fe}_{15.48}\text{Al}_{1.34}\text{O}_{28}$ (s), with the general formula of $\text{M}_{20}\text{O}_{28}$, which is consistent with SFCA-I. SFCA-I has low levels of SiO_2 in its crystal structure.^[9,10] Ti^{+4} and Si^{+4} might have also replaced some Fe^{3+} in the calcium ferrite phase, to yield $3\text{CaO}\cdot \text{Fe}_2\text{O}_3\cdot \text{Si}_{1.58}\text{Ti}_{1.42}\text{O}_6$ (s). $\text{TI}_{+2 \text{ mm}}$ and $\text{RDI}_{+2 \text{ mm}}$ results indicate that sinter formed using blend 1 had better sinter strength than sinters formed by using blends 2 through 6 (Figure 3). SFCA-I imparts high strength in sinter,^[9,10] so the presence of SFCA-I as one of the phases in this sinter might have greatly improved the bonding strength.

Addition of ilmenite ore to the hematite ore formed $4\text{CaO}\cdot 7\text{Fe}_2\text{O}_3$ (s) (ICDD 00-013-0342), $2\text{FeO}\cdot \text{SiO}_2$ (s) (ICDD 00-009-0484), $\text{Fe}_{2.95}\text{Si}_{0.05}\text{O}_4$ (s) (ICDD 00-052-01140), and $3\text{CaO}\cdot \text{Fe}_2\text{O}_3\cdot \text{Si}_{1.58}\text{Ti}_{1.42}\text{O}_6$ (s) (ICDD 01-078-0319) as components of the bonding phases (Figure 4(b)). The ilmenite ore had high levels of magnetite (Fe_3O_4 (s)) as one of the major phases (Figure 1). An increase in Fe_3O_4 (s) in sinter was reported to stabilize the $2\text{FeO}\cdot \text{SiO}_2$ (s) phase.^[15] In addition, increasing Fe_3O_4 (s) might have increased the probability of the solid-state reaction between Fe_3O_4 (s) and SiO_2 (s) to yield $2\text{FeO}\cdot \text{SiO}_2$ (s).^[3] Addition of ilmenite into the hematite ore might have led to the formation of SFCA, which decreased the mechanical properties of the sinter as compared to that of blend 1 that had some SFCA-I as one of the bonding phases.

Addition of magnetite to hematite influences the melting behavior as well as the melt properties.^[15] Ilmenite ore has magnetite as one of the major phases, so the melting temperature of the sinter blend might have been increased and this change might affect the assimilation of the Al and Si into the calcium ferrites during the formation of SFCA.

The increase in Ti as a result of the addition of ilmenite might have increased the amount of Ti in the calcium ferrite phase; this change might increase the structural stress in the sinter, affecting its mechanical properties. Results from EDS and EPMA were acquired to determine the location of Ti within the bonding phases.

An increase in the ilmenite addition in blend 3 resulted in the formation of $5\text{CaO}\cdot \text{FeAlO}_3\cdot 4\text{Fe}_2\text{O}_3\cdot 4\text{Al}_2\text{O}_3\cdot 2\text{SiO}_2$ (s) (ICDD 00-033-0250), $3\text{CaO}\cdot \text{FeO}\cdot 7\text{Fe}_2\text{O}_3$ (s) (ICDD 00-021-0916), and $12\text{CaO}\cdot 7\text{Al}_2\text{O}_3$ (s) (ICDD 00-048-1882) as the major bonding phases (Figure 4(c)). Addition of ilmenite increased the Fe_3O_4 (s) content in this blend; this change might have led to the development of $3\text{CaO}\cdot \text{FeO}\cdot 7\text{Fe}_2\text{O}_3$ (s). Under reducing conditions, some ferrites that contain FeO, especially $\text{FeO}\cdot \text{CaO}\cdot \text{Fe}_2\text{O}_3$, formed during sintering.^[13] The

increase in ilmenite in the sinter blend might have also increased the Al_2O_3 content in the sinter blend, which might have resulted in the formation of $12\text{CaO}\cdot 7\text{Al}_2\text{O}_3$ (Figure 4(c)).

In blend 4, $5\text{CaO}\cdot \text{FeAlO}_3\cdot 4\text{Fe}_2\text{O}_3\cdot 4\text{Al}_2\text{O}_3\cdot 2\text{SiO}_2$ (s) (ICDD 00-033-0250), $\text{CaO}\cdot \text{TiO}_2$ (s) (ICDD 00-042-0423), $\text{MgO}\cdot \text{Fe}_2\text{O}_3$ (s) (ICDD 00-017-0465), and Fe_3O_4 (s) (ICDD 01-089-0691) composed part of the bonding phases that formed during sintering (Figure 4(d)). $\text{CaO}\cdot \text{TiO}_2$ (s) was identified in the same peak position as Fe_2O_3 (s), and also as an independent peak. The $\text{CaO}\cdot \text{TiO}_2$ (s) might have existed in the same area as the Fe_2O_3 (s)-enriched area. Further increase in ilmenite (Figure 4(e)) resulted in the formation of $\text{CaO}\cdot \text{FeO}\cdot 2\text{SiO}_2$ (s) (ICDD 00-041-1372), $\text{CaO}\cdot \text{TiO}_2\cdot \text{SiO}_2$ (s) (ICDD 01-073-2066), $2\text{CaO}\cdot \text{SiO}_2$ (s) (ICDD 00-029-0371), and $\text{MgO}\cdot \text{Fe}_2\text{O}_3$ (s) (ICDD 01-089-3084) as part of the bonding phases (Figure 4(e)).

Addition of ilmenite ore might have increased the Ti content in the sinter blend leading to the formation of $\text{CaO}\cdot \text{TiO}_2$ (s) and $\text{CaO}\cdot \text{TiO}_2\cdot \text{SiO}_2$ (s) phases that were identified in the sinters made from blends 4 and 5. In previous results,^[1,5] Ti was distributed in the glass phase and weakened the bonding phase. TiO_2 (s) reacts with CaO from molten SFCA, resulting in the formation of Fe_2O_3 (s), $\text{CaO}\cdot \text{TiO}_2$ (s), and $2\text{CaO}\cdot \text{SiO}_2$ (s).^[2] The phase change of $2\text{CaO}\cdot \text{SiO}_2$ (s) from β - $2\text{CaO}\cdot \text{SiO}_2$ to γ - $2\text{CaO}\cdot \text{SiO}_2$ during cooling of sinter causes some volume expansion, which might have resulted in the weakening of sinter strength and in generating cracks.^[4,13] The internal part of the sinter contains Fe_2O_3 (s), and RDI deterioration might have been caused by the volume expansion from the reduction of the exposed Fe_2O_3 (s).^[1,2] The $2\text{CaO}\cdot \text{SiO}_2$ (s) phase was identified in the sinter made from blend 5 (Figure 4(e)), and this sinter recorded both the lowest $\text{TI}_{+2 \text{ mm}}$ and the RDI (Figure 3).

Sintered blend 6 consists of $\text{CaO}\cdot \text{Fe}_{1.4}\text{Al}_{0.6}\text{O}_3\cdot \text{SiO}_2$ (s) (ICDD 00-025-0143), $\text{CaO}\cdot \text{FeO}\cdot 2\text{SiO}_2$ (s) (ICDD 00-041-1372), $\text{CaO}\cdot \text{FeO}\cdot \text{SiO}_2$ (s) (ICDD 00-011-0477), $\text{CaO}\cdot \text{TiO}_2\cdot \text{SiO}_2$ (s) (ICDD 01-073-2066), and $\text{MgO}\cdot \text{Fe}_2\text{O}_3$ (s) (ICDD 00-036-0398) as the bonding phases. Low strength in the sinter made from blend 6 might have resulted from the increased porosity caused by the presence of a relatively large amount of more MgO ^[16] as well as the presence of $\text{CaO}\cdot \text{TiO}_2\cdot \text{SiO}_2$ (s). However, results from optical microscope should be obtained to access whether porosity did increase.

Addition of ilmenite up to 25 wt pct, blend 6, slightly improved $\text{RDI}_{+2 \text{ mm}}$ and $\text{TI}_{+2 \text{ mm}}$ (Figure 3). Addition of 6 to 12 wt pct TiO_2 (s) improved the RDI of chromium-bearing vanadium titanomagnetite. The result was attributed to homogeneous distribution of $\text{CaO}\cdot \text{TiO}_2$ (s) in the silicate phase^[8]; the sinters also showed $2\text{MgO}\cdot \text{TiO}_2$ (s) phase. The bonding strength was increased slightly in the sinter made from blend 6 (Figure 3). Addition of ilmenite to hematite ore causes an increase in TiO_2 (s) content and might, thereby, increase the amount $\text{CaO}\cdot \text{TiO}_2$, which degrades the bonding strength; however, the opposite effect was observed in this sinter. The difference may have occurred because addition of ilmenite to the sinter mix

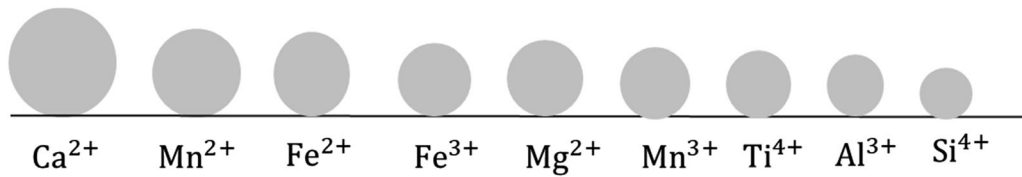


Fig. 5—Relative size of different cations (pm) (reprinted with permission from Ref. [6]).

caused an increase in the amount of MgO (Table IV), which provides Mg^{2+} that can replace Fe^{2+} in $\text{FeO}\cdot\text{TiO}_2$ (s) and Fe_3O_4 (s) to instead yield $2\text{MgO}\cdot\text{TiO}_2$ (s) or $\text{MgO}\cdot 2\text{TiO}_2$ (s) or $\text{MgO}\cdot\text{Fe}_2\text{O}_3$ (s).^[8] The ionic radii of Fe^{2+} (92 pm) and Mg^{2+} (86 pm) are comparable (Figure 5),^[3] so Mg^{2+} can easily replace Fe^{2+} in $\text{FeO}\cdot\text{TiO}_2$ (s) without affecting the crystal structure. This process might have decreased the amount of TiO_2 (s) that was available for formation of $\text{CaO}\cdot\text{TiO}_2$ (s).

It can be clearly seen (Figure 5) that the replacement of Fe^{2+} with Mg^{2+} can occur since the cationic sizes are almost similar. The previous research^[3] has shown that Mg^{2+} and Al^{3+} are more likely to diffuse into Ti-rich Fe phases, while the diffusion of Ca^{2+} into the Ti-rich Fe phase was found to be low, probably due to its large ionic size.^[3] That is, Mg^{2+} can replace Fe^{2+} while Al^{3+} can replace Fe^{3+} . The Ti^{4+} and Si^{4+} might also replace the Fe^{3+} ions, as evidenced by the XRD results of sintered blends 1 and 2, which showed the presence of the $3\text{CaO}\cdot\text{Fe}_2\text{O}_3\cdot\text{Si}_{1.58}\text{Ti}_{1.42}\text{O}_6$ (s) (Figures 4(a) and (b)).

To further investigate the bonding phases formed, EDS analysis was done on sintered, mounted, and polished samples made from blends 1 through 6 (Figures 6(a) through (f), Tables V through X). In calculating the atomic percentages, residual carbon in the selected points was ignored.

In sintered blend 1 (Figure 6(a) and Table V), which lacked ilmenite, the main bonding phases were likely to be the SFCA, iron silicates, and iron silicate aluminates. The Ti was likely to be within the SFCA phase. XRD results showed the possible presence of SFCA-I ($\text{Ca}_{3.18}\text{Fe}_{15.48}\text{Al}_{1.34}\text{O}_{28}$ (s); general formula of $\text{M}_{20}\text{O}_{28}$) and that the Ti was in the $3\text{CaO}\cdot\text{Fe}_2\text{O}_3\cdot\text{Si}_{1.58}\text{Ti}_{1.42}\text{O}_6$ (s) phase.

In blend 2, the addition of ilmenite resulted in the formation of SFCA with increased amount of Ti in the SFCA structure (Figure 6(b) and Table VI). The iron silicate was part of the bonding phase; this result concurs with the XRD results, which detected the presence of fayalite (Figure 4(b)).

In blend 3 (Figure 6(c) and Table VII), the sinter had SFCA as one of the bonding phases; XRD results (Figure 4c) showed $5\text{CaO}\cdot\text{FeAlO}_3\cdot 4\text{Fe}_2\text{O}_3\cdot 4\text{Al}_2\text{O}_3\cdot 2\text{SiO}_2$ (s) as one of the bonding phases, and EDS results showed that the Mg-enriched SFCA was also part of the bonding phase. The amount of Ti in both SFCA and

Mg-enriched SFCA increased greatly (Table VII). MgO might have stabilized Ti in the SFCA. The sinter strength was lower in sintered blends 2 and 3 than in sintered blend 1; the difference might be ascribed to an increase in Ti in the SFCA in blend 2 (Table VI) and blend 3 (Table VII). SFCA rich in Ti had more Mg than Ca (Table VII); this difference shows the ion-size advantage of Mg^{2+} ions over Ca^{2+} and supports the predictions based on Figure 5.

The XRD results (Figure 4(a)) indicated that the sintered blend 1 might have had some SFCA-I as part of the bonding phase. This suggests that the sintered blend 1 has better properties than the other sintered blends. The presence of large amounts of Ti in the SFCA of sintered blends 2 and 3 might cause an increase in structural stress and weaken the bonding phase. However, the effects of MgO and Ti on the formation of SFCA must be further studied.

In blend 4, The EDS results (Figure 6(d) and Table VIII) suggested the existence of Ti-enriched SFCA, Mg-enriched SFCA, and some Ti-enriched iron aluminum silicates. The XRD results (Figure 4(d)) for this blend indicate that the $5\text{CaO}\cdot\text{FeAlO}_3\cdot 4\text{Fe}_2\text{O}_3\cdot 4\text{Al}_2\text{O}_3\cdot 2\text{SiO}_2$ (s) was one of the bonding phases formed, and the $\text{CaO}\cdot\text{TiO}_2$ peaks were identified in the same position as Fe_2O_3 ; this coincidence shows the possibility that Ti can enter the Fe-enriched region. To clarify the formation of $\text{CaO}\cdot\text{TiO}_2$, more results from EPMA mapping are required.

In blend 5 (Figure 6(e) and Table IX), XRD showed the presence of the $\text{CaO}\cdot\text{FeO}\cdot 2\text{SiO}_2$ (s) (Figure 4(e)); this result suggests that the bonding phase might be the iron calcium silicate. EDS results also suggested the possible existence of Ti-enriched iron silicate aluminate phase. The XRD showed that in this blend, Ti might exist in the $\text{CaO}\cdot\text{TiO}_2\cdot\text{SiO}_2$ (s) phase; more EPMA mapping results could test this suggestion.

In blend 6 (Figure 6(f) and Table X), the bonding phase might be some Ti-enriched SFCA, Mg- and Ti-enriched SFCA, and some iron calcium silicate aluminate rich in Ti. The XRD analyses of this sinter blend (Figure 4(f)) showed the possible presence of $\text{CaO}\cdot\text{Fe}_{1.4}\text{Al}_{0.6}\text{O}_3\cdot\text{SiO}_2$ (s), which might concur with EDS results. The Mg-enriched SFCA contained a large amount of Ti and some V; this result suggests that Mg has the potential to stabilize Ti in the Fe-enriched phase

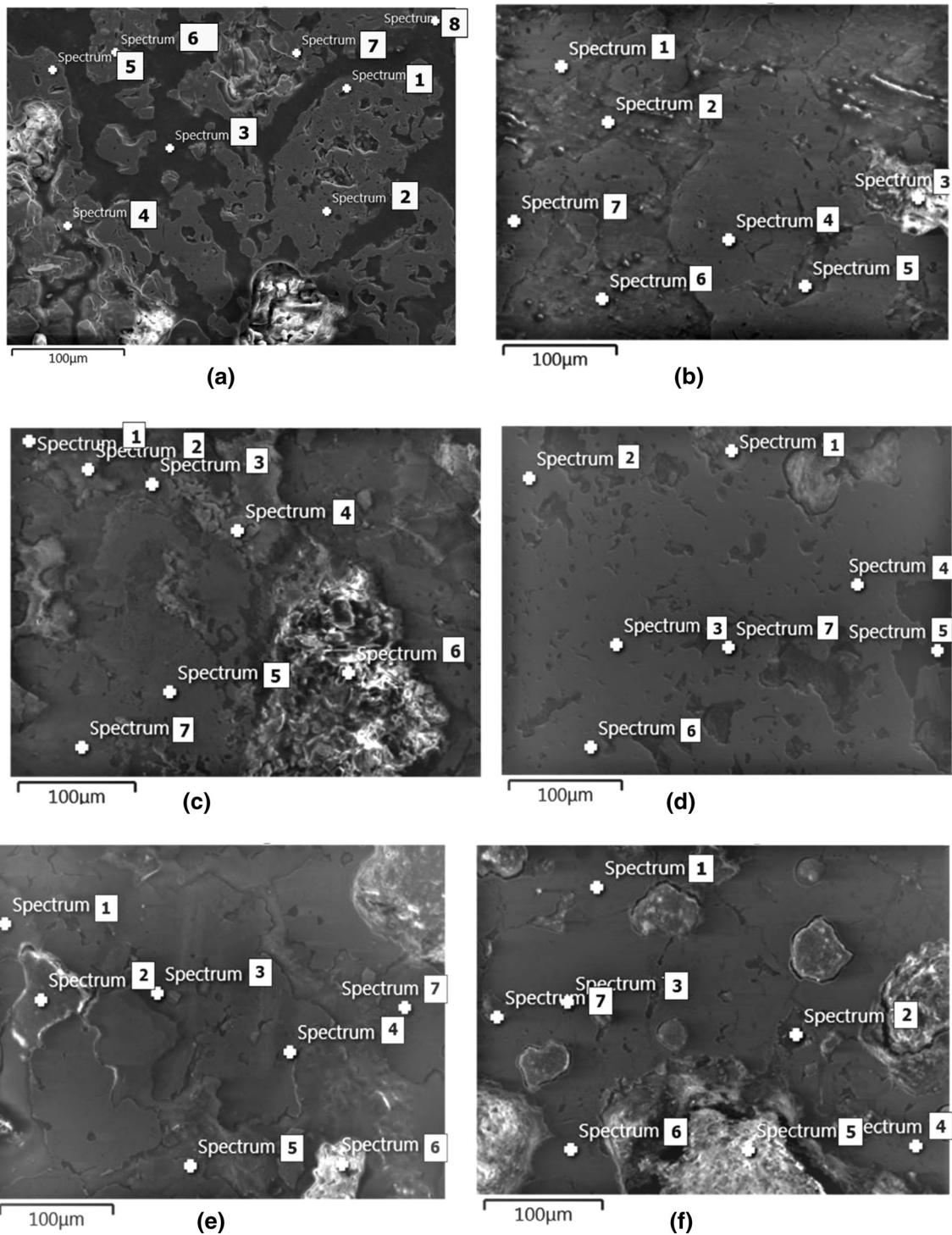


Fig. 6—EDS analysis of (a) sintered blend 1, (b) sintered blend 2, (c) sintered blend 3, (d) sintered blend 4, (e) sintered blend 5, and (f) sintered blend 6.

by forming some complicated phases. Further research using high-temperature *in-situ* XRD might improve understanding of this phenomenon.

The EDS results of sintered blends 2 through 5 (Tables VI through X) showed some points with high Fe and Si but no O. These points contained high levels of C; this result suggests that Fe and Si existed as carbides.

C. Elemental Distribution with Increasing Ilmenite Addition

Polished samples of the sinters made from blends 1 through 6 were analyzed using EPMA to confirm Ti distribution after sintering. The EPMA results of sinters from blends 1 through 3 confirmed XRD results that perovskite did not form (Figures 4(a) through (c)). The

Table V. EDS Analyses of Sintered Blend 1

Point	Atomic Percent					
	Fe	Ca	Al	Si	Ti	O
1	32.04	0.30	0.50	0.13	—	67.04
2	28.65	0.81	1.05	0.28	0.08	69.13
3	3.98	—	—	17.23	—	78.79
4	47.19	0.21	0.38	0.46	—	51.77
5	26.09	2.19	0.80	1.27	—	69.66
6	38.12	—	0.29	4.78	—	56.81
7	43.43	0.37	0.24	3.61	0.20	52.15
8	37.14	—	0.51	0.19	0.10	62.03

Table VI. EDS Analyses of Sintered Blend 2

Point	Atomic Percent						
	Fe	Ca	Al	Si	Ti	S	O
1	34.96	—	0.51	0.17	0.16	—	64.20
2	6.58	—	—	32.12	—	1.74	59.56
3	15.63	—	—	41.94	—	—	42.43
4	35.14	0.10	0.42	0.23	0.20	—	63.92
5	72.63	—	—	27.37	—	—	—
6	4.88	—	—	31.59	—	—	63.53
7	34.08	0.12	0.39	0.25	0.30	—	64.62

Table VII. EDS Analyses of Sintered Blend 3

Point	Atomic Percent						
	Fe	Ca	Al	Si	Ti	Mg	O
1	32.46	0.09	0.45	0.26	0.49	—	66.26
2	60.21	—	—	39.79	—	—	—
3	17.72	2.56	5.65	2.69	1.61	4.06	65.87
4	24.34	0.07	1.36	0.58	4.59	4.03	65.06
5	24.96	0.06	1.21	0.78	2.79	2.20	68.02
6	0.30	1.26	—	15.66	—	—	82.77
7	32.10	0.07	0.78	0.27	0.58	—	66.19

Table VIII. EDS Analyses of Sintered Blend 4

Point	Atomic Percent						
	Fe	Ca	Al	Si	Ti	Mg	O
1	2.03	0.26	0.29	6.81	—	—	90.62
2	25.00	5.90	1.53	1.99	—	1.16	64.44
3	31.35	0.32	0.58	—	1.32	—	66.42
4	30.75	—	0.57	0.07	0.57	—	68.02
5	94.21	—	—	5.79	—	—	—
6	32.50	0.16	0.56	0.12	0.63	—	66.02
7	32.73	—	0.57	0.11	0.83	—	65.76

TiO₂ (s) content in these sinter blends was too low to form detectable amounts of CaO·TiO₂ (s); instead, the small amounts of TiO₂ (s) were evenly distributed in the iron-rich phase (Figures 7(a) through (c)). The EDS and XRD of sinter blends 1 through 3 results also showed that the Ti could exist in the SFCA, whereas Al and Ca were distributed in the iron-rich phase; this observation indicates that SFCA may be present. The XRD results (Figure 4(a)) of the sintered blend 1 showed that SFCA-I might be present. Bristow *et al.*^[1] reported that most of CaO·TiO₂ (s) was distributed in the glass phase, affecting the physical properties of sinter. Most of Ti was distributed in the same region as Ca, Al, and Si (Figures 7(d) and (e)); this result suggests that in these sinters, Ti might occur in the glass phase. The Ti-rich area was in the same region as the Ca-rich area (marked area in Figure 7(d)); this coincidence suggests that the CaO·TiO₂ phase formed in this sinter. However, with a further increase in ilmenite addition (Figure 7(f)), most of the Ti became distributed in the Fe-rich region, possibly as a result of interaction with MgO (s). An increase in ilmenite addition caused MgO (s) content to increase, and this change could have led to formation of complicated phases, such as MgO·Fe₂O₃·3TiO₂ (s), which might stabilize Ti in the Fe-rich phase. EDS results (Tables VII and X) showed that Ti existed preferentially in the Mg-rich Fe-bearing phases. Mg²⁺ can replace Fe²⁺,^[3] and this process may stabilize Ti in Fe-rich phases. This phenomenon can complicate the release mechanism of TiO₂ (s); this possibility should be investigated. Vanadium was also distributed preferentially in the Fe-rich region (Figure 7(f)); this result concurs with the EDS results (Table X).

D. Morphological Change with Increasing Ilmenite Addition

The morphological change with increasing ilmenite addition (Figures 8(a) through (f)) was investigated using an optical microscope (Leica DM 4000M) to confirm the bonding phases formed. Sintered blend 1 included some intersecting fibers (Figure 8(a)); this observation suggests that this sinter might include some SFCA-1. XRD results (Figure 4(a)) confirmed this possibility.

The sinters of the blends showed different morphologies. The sinter made from blend 1 generated the lowest number of fines, as evidenced by RDI_{+2 mm}. This result is sufficient evidence that SFCA-1 has better bonding properties than the other bonding phases. Sintered blend 2 contained some big platelike columnar morphology. Sintered blend 3 had small columnar morphology with improved porosity in between the columns (Figures 8(b) and (c)); this observation suggests that SFCA might have been part of the bonding phase in the sintered blends. XRD results (Figure 4(b)) identified that sintered blend 2 includes 4CaO·7Fe₂O₃ (s), whereas sintered blend 3 consists of 3CaO·FeO·7Fe₂O₃ (s), which might result in some columnar morphology. EDS

Table IX. EDS Analyses of Sintered Blend 5

Point	Atomic Percent							
	Fe	Ca	Al	Si	Ti	Mg	S	O
1	83.32	—	—	16.68	—	—	—	—
2	2.45	0.25	0.36	14.07	—	—	13.23	69.61
3	20.87	—	2.06	6.97	2.13	—	—	67.97
4	27.48	—	1.14	2.49	1.45	—	—	67.45
5	28.87	—	1.35	0.47	1.06	—	—	68.25
6	0.80	0.11	0.13	7.56	—	—	2.34	89.05
7	29.14	—	1.70	0.22	1.77	—	—	67.17

Table X. EDS Analyses of Sintered Blend 6

Point	Atomic Percent								
	Fe	Ca	Al	Si	Ti	Mg	V	S	O
1	66.77	14.03	—	19.20	—	—	—	—	—
2	19.08	0.09	7.76	0.14	5.15	1.26	0.18	—	66.34
3	28.00	0.11	2.35	0.35	3.83	—	0.19	—	65.17
4	33.12	—	0.53	0.25	1.23	—	—	—	64.87
5	4.65	—	—	2.23	—	—	—	1.44	91.68
6	30.06	1.35	0.44	1.60	0.13	—	—	—	66.41
7	3.18	0.35	0.37	9.17	—	—	—	4.87	82.06

(Tables VI and VII) suggests the possibility that SFCA formed in these sinters. Sintered blends 4 and 5 (Figures 8(d) and (e)) had complex morphologies, possibly as a result of the presence of $\text{CaO}\cdot\text{TiO}_2$ (s), which affected the generation of the SFCA. Sintered blend 6 (Figure 8(f)) showed a columnar morphology. EDS results (Table X) indicate that SFCA might be one of the bonding phases in sintered blend 6; this inference concurs with the XRD results (Figure 4(f)), which indicate the presence of $\text{CaO}\cdot\text{Fe}_{1.4}\text{Al}_{0.6}\text{O}_3\cdot\text{SiO}_2$ (s).

E. Melt Formation Temperature with Increasing Ilmenite Addition

The melt formation temperature was estimated by a DSC using the heat flow. The typical DSC curves of the sinter blend were as shown subsequently (Figure 9(a)).

Blend 1 is composed mainly of hematite ore with a basicity (CaO/SiO_2) of 2. The first bonding phase formed in this sinter is likely to be calcium ferrites formed by solid-state reaction, which starts at 750 °C to 780 °C.^[17] The melting temperature of these calcium ferrites is ~ 1200 °C.^[17] Melting is an endothermic process. Closer inspection of the trend for sintered blend 1 shows a trough at ~ 1200 °C (Figure 9(a)), which might be ascribed to the melting of these calcium ferrites. Enlarging of DSC peaks of all the sintered blends in between 1100 °C and 1300 °C allowed estimation of the temperature at which melt forms in each sintered blend (Figure 9(b)).

The melting temperature of blend 1 was estimated to be 1186 °C (Figure 9(b)). The phase diagrams of $\text{CaO}\text{-SiO}_2\text{-Fe}_2\text{O}_3$ and $\text{CaO}\text{-Al}_2\text{O}_3\text{-Fe}_2\text{O}_3$ indicate that the presence of a small amount of SiO_2 (s) and Al_2O_3 (s) decreased the solidus temperature of the first melt in the sintering of high-grade hematite ore to a range between 1175 °C and 1192 °C,^[18] which includes our estimate.

The addition of ilmenite increased the melting point of the sinter blends (Figure 9(c)); this trend can be explained by two factors. Increasing ilmenite addition caused an increase in the magnetite (Fe_3O_4 (s)) content in the resulting sinter mix. Addition of magnetite to hematite affected the melting behavior and melt properties of the mixture.^[15] The second possibility is that the increased TiO_2 (s) content in the sinter blends may have resulted in formation of $\text{CaO}\cdot\text{TiO}_2$ (s), which has a high melting temperature.

When 15 wt pct ilmenite was added (blend 4), the XRD analysis results (Figure 4(d)) identified the presence of $\text{CaO}\cdot\text{TiO}_2$ (s) and $\text{MgO}\cdot\text{Fe}_2\text{O}_3$ (s), which have high melting temperature. Addition of >15 wt pct ilmenite might have increased the content of other metallic components in the sinter, and these may have interacted with the release mechanism of the TiO_2 (s) from the $\text{FeO}\cdot\text{TiO}_2$ (s) to form $\text{CaO}\cdot\text{TiO}_2$ (s). This phenomenon increased the possibility of forming $\text{CaO}\cdot\text{FeO}\cdot 2\text{SiO}_2$ (s), which was identified by XRD in sintered blends 5 and 6 (Figures 4(e) and (f)). Sintered blend 6 also includes $\text{CaO}\cdot\text{Fe}_{1.4}\text{Al}_{0.6}\text{O}_3\cdot\text{SiO}_2$ (s), which is a derivative of calcium ferrite, which has a relatively low

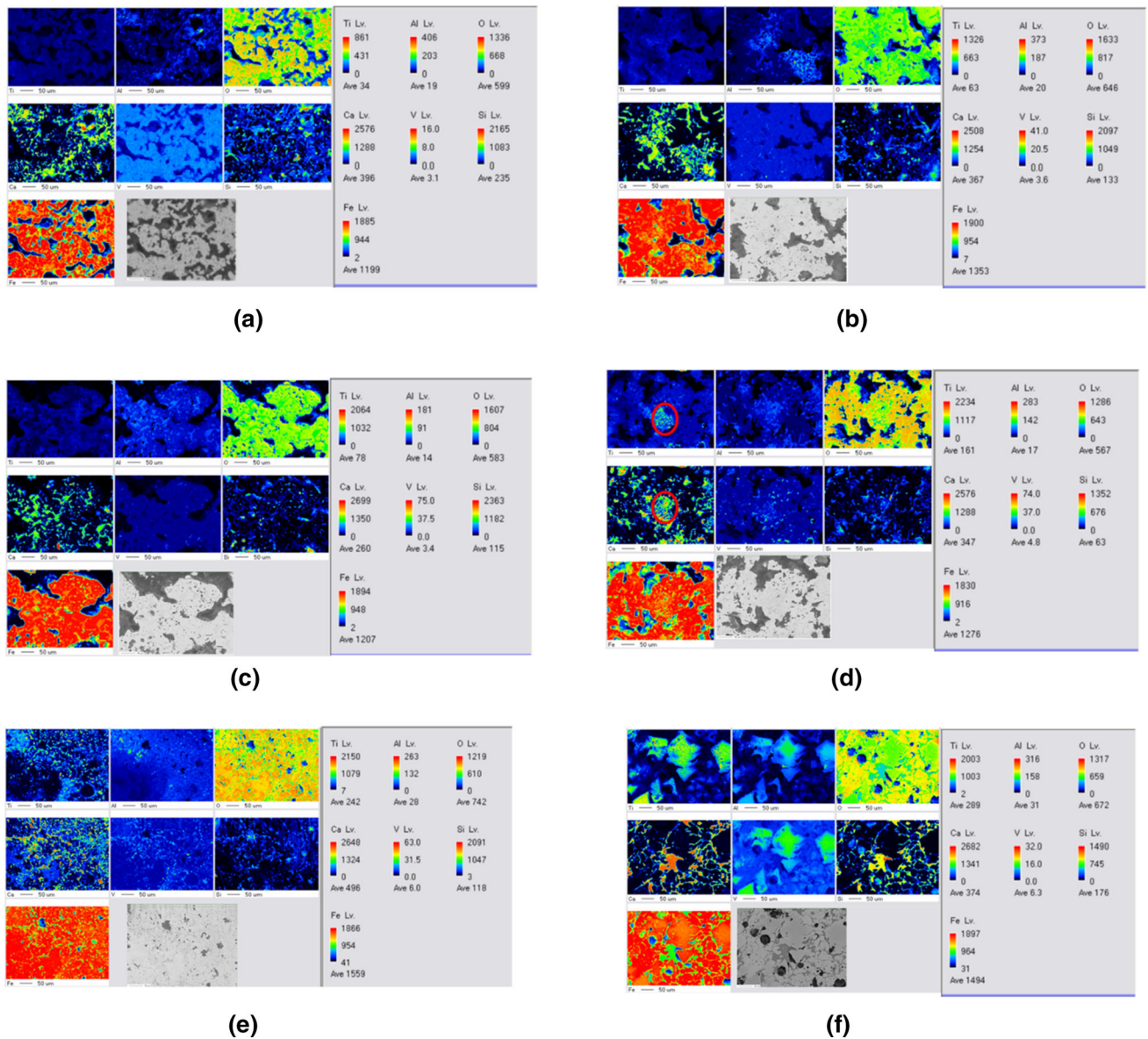


Fig. 7—(a) through (f) Element distribution of sintered blends based on the EPMA: (a) hematite only, (b) 5 wt pct addition, (c) 10 wt pct addition, (d) 15 wt pct addition, (e) 20 wt pct addition, and (f) 25 wt pct addition.

melting point. The EDS results (Table X) indicate that SFCA rich in Mg might contain more Ti in the SFCA crystal structure; this possibility suggests that Ti might be stabilized by Mg in SFCA.

Development of sinter bonding phases may involve several stages.^[19] First, some phases that have low melting points appear in a solid-state reaction, and then secondary liquid phases form as the temperature increases. Progressively more liquid phases are generated and polymerized because of the solution behavior between the primary liquid phase and sintering material. Finally, during cooling, the sinter strength is improved by agglomeration of sinter by the bonding phase.^[19] Thus, generation of the liquid phase is of extreme importance in the development of bonding phases in the sinter. If the temperature of melt formation increases,

the amount of liquid phase formed is likely to decrease. An increase in ilmenite addition to the hematite sinter blends increased the melt formation temperature (Figure 9(c)), so the amount of melt decreased and the sinter developed poor bonding strength. The improvement of the sinter strength at 25 wt pct addition could have resulted from improved liquid generation because of the lowered temperature of melt formation.

The reason for the lowered melting temperature may be a result of interference of Mg^{2+} ions by sequestering TiO_2 by formation of complex phases; this process would decrease the amount of reactive TiO_2 (s) in the system and thereby reduce the amount of $CaO \cdot TiO_2$ (s) that formed. In this experiment, TiO_2 (s) was introduced into the sinter blends in the form of $FeO \cdot TiO_2$ (s). Diffusion of Ti^{4+} from the iron-rich phase into MgO or

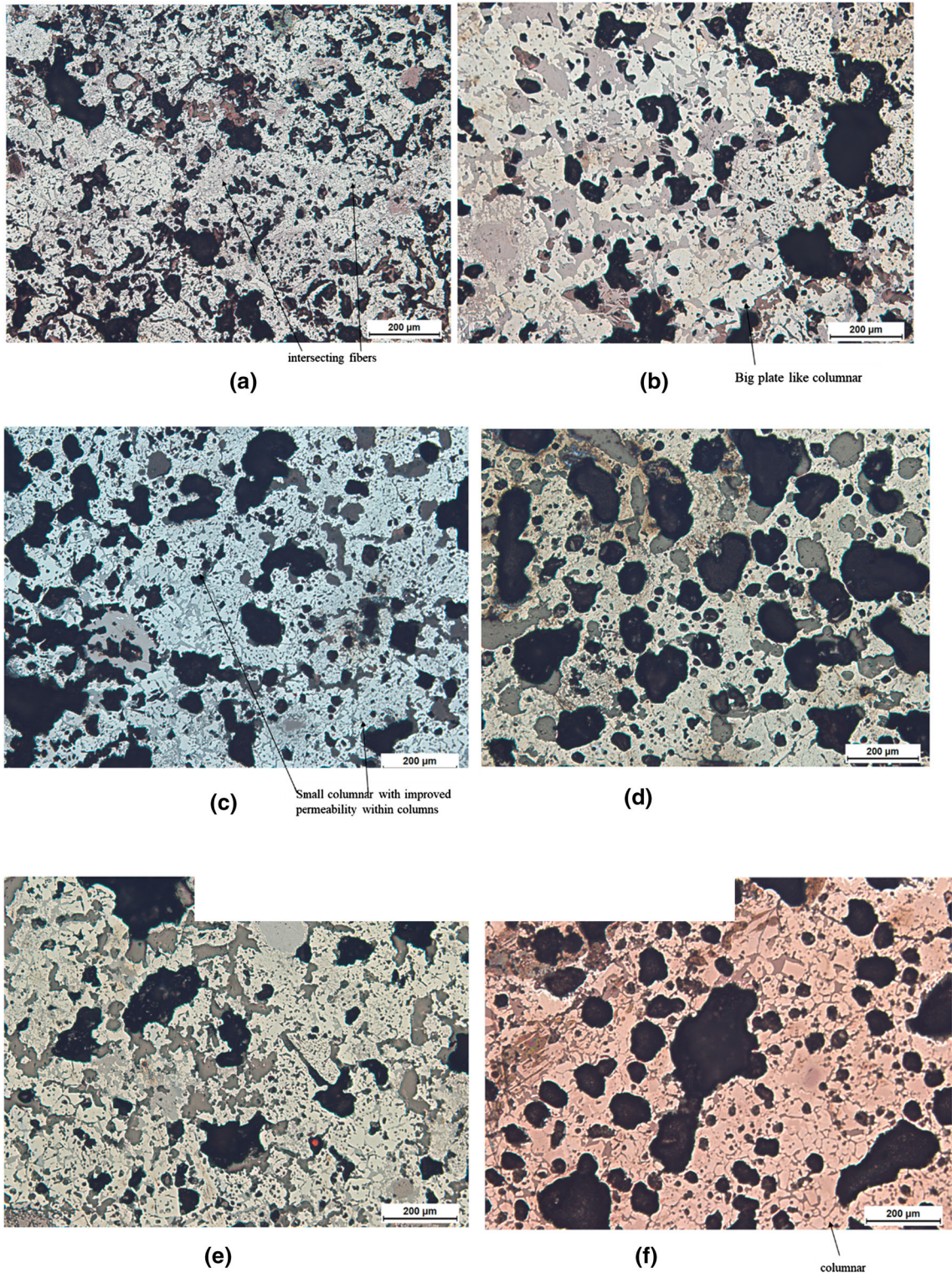


Fig. 8—(a) through (f) Morphological changes with increasing ilmenite addition: (a) hematite ore only, (b) 5 wt pct addition, (c) 10 wt pct addition, (d) 15 wt pct addition, (e) 20 wt pct addition, and (f) 25 wt pct addition.

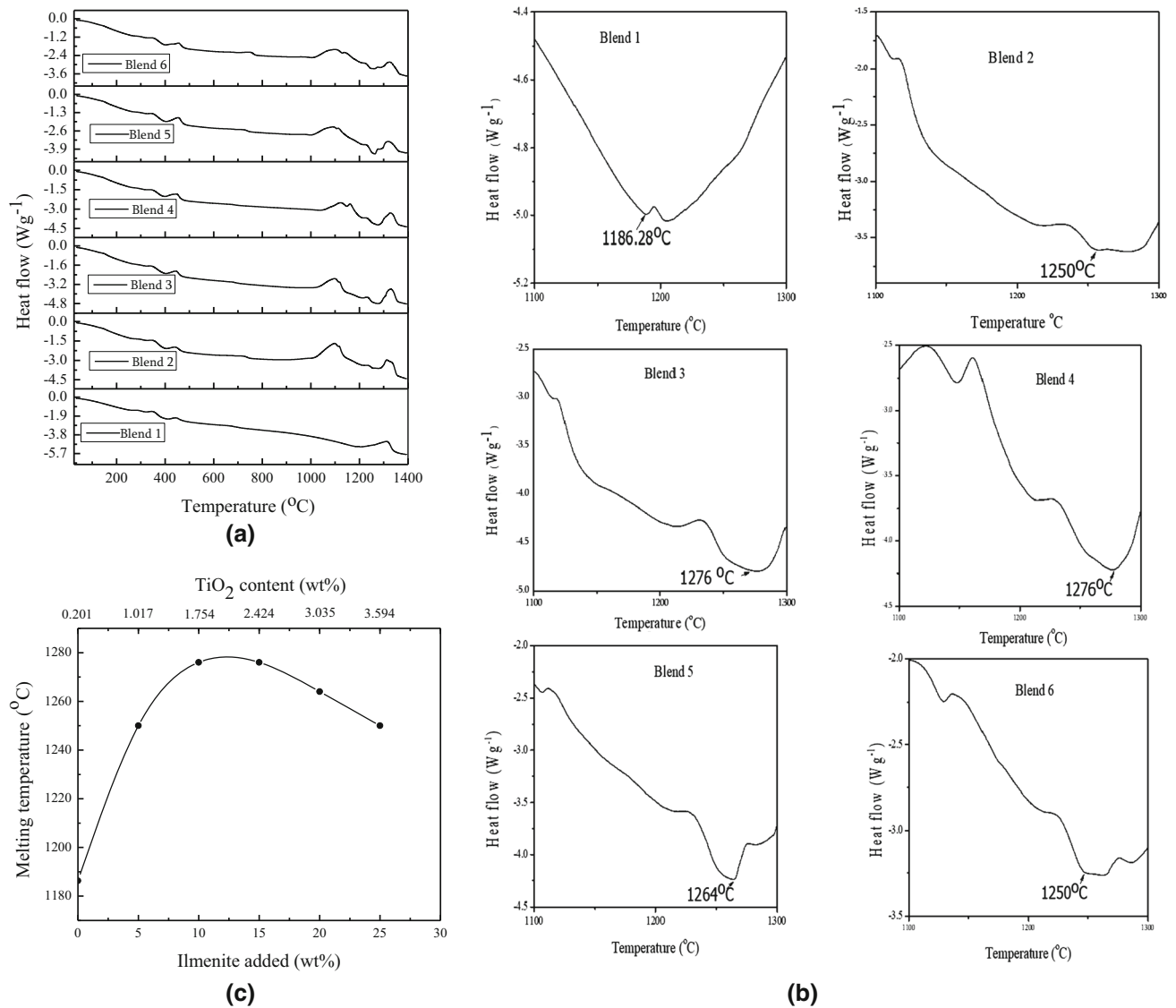
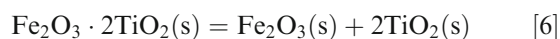
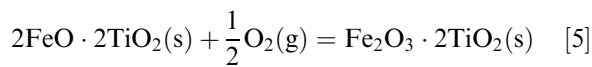


Fig. 9—(a) Typical DSC curves of the sinter blends in argon atmosphere. (b) Estimation of melt formation temperature of the sinter blends using the heat flow in the DSC method in argon atmosphere. (c) Melt formation temperature curve with increase in ilmenite ore addition determined by the DSC method in inert atmosphere.

CaO is low^[3]; therefore, the formation of CaO·TiO₂ (s) might require that the FeO·TiO₂ (s) phase release TiO₂ (s) into a reactive form. The release of TiO₂ (s) from FeO·TiO₂ (s) during sintering occurs according to the following reactions^[20–22]:



The presence of Mg²⁺ ion in the system can impede the release of TiO₂ (s) and, thereby, decrease the amount available for formation of CaO·TiO₂ (s). However, to clarify the actual effect of other metallic elements, such as MgO, the formation mechanism of CaO·TiO₂ (s)

must be determined. High-temperature *in-situ* XRD might facilitate the clarification of the mechanism providing useful knowledge about this phenomenon.

F. CaO-Fe₂O₃-TiO₂ Phase Diagram

An attempt was made to fit the current data into a CaO-Fe₂O₃-TiO₂ ternary phase diagram^[4] (Figure 10). The phase marked “magnetite” on the phase diagram is believed to be composed of titanomagnetite, whereas that marked “hematite” contains titanohematite.^[4] The basicity (CaO/SiO₂) of the blends had been adjusted to 2, so in fitting the current data into the phase diagram, each sinter blend was assumed to have enough CaO to allow formation of CaO·TiO₂ (s). All of the sinter blends contain hematite ore, so the major phase was Fe₂O₃. Therefore, the limiting factor for the generation of CaO·TiO₂ (s) was the availability of TiO₂ (s). Hence, the

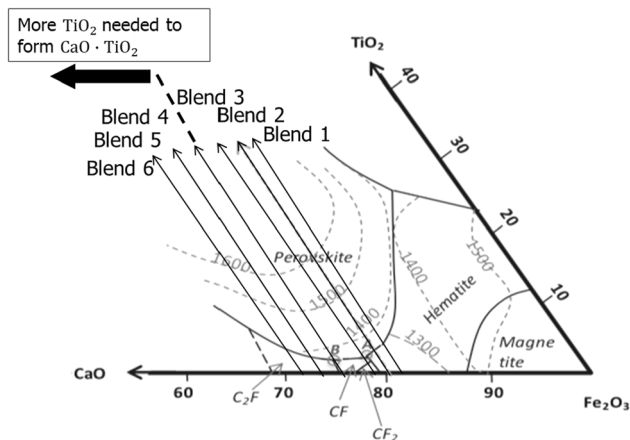


Fig. 10—Projection of the liquidus surface of the CaO-Fe₂O₃-TiO₂ ternary phase diagram (adapted from Ref. [4]) with the position of each sinter blend marked from 1 through 6.

location of each sinter blend was estimated on the phase diagram by considering only the Fe₂O₃ (s) and TiO₂ (s) contents. The phase diagram demonstrates that CaO-TiO₂ (s) was not expected in sinters made from blends 1 through 3, because their TiO₂ (s) content was too low; the Ti was expected to be in the calcium ferrite phase. This inference was confirmed by XRD results (Figures 4(a) and (b)), which showed the presence of 3CaO·Fe₂O₃·Si_{1.58}Ti_{1.42}O₆ (s), which is a derivative of calcium ferrite, whereas EPMA results (Figures 7(a) through (c)) showed that the Ti was distributed in areas that were rich in Fe, Ca, and Si.

Sintered blend 1 had SFCA-I as one of the main bonding phases (Figure 4(a)), and sintered blend 2 had 4CaO·7Fe₂O₃ (s) as one of the bonding phases (Figure 4(b)). The phase diagram predicts the formation of CaO·2Fe₂O₃ (s) as the main bonding phase in the sinter from blend 2. However, current results also showed the presence of other bonding phases in this sinter, other than those predicted by the phase diagram; this result occurs because the increase in ilmenite content in the sinter blend also increased the content of other components, such as SiO₂ and Al₂O₃, in the sinter mix. The presence of Fe₃O₄ (s) might have resulted in formation of 3CaO·FeO·7Fe₂O₃ (s) in sinter from blend 3, but CaO·Fe₂O₃ (s) was expected to be the main bonding phase according to the phase diagram. Blend 4 has enough TiO₂ to allow formation of CaO·TiO₂, which is estimated to require about 2 wt pct TiO₂, as predicted by the phase diagram. This result indicates that formation of CaO·TiO₂ (s) is possible in the sinters made from blends 4 through 6, which contained > 2 wt pct TiO₂.

G. Effect of Ilmenite Addition on Hematite Ore Reduction

The reduction degree was affected by increasing ilmenite addition in the sinter (Figure 11). The difference in the reduction behavior of the sinter might be related to the type of phases that form during the sintering process and to the physical properties of the sinter.^[13] The total porosity of the sinter varied slightly

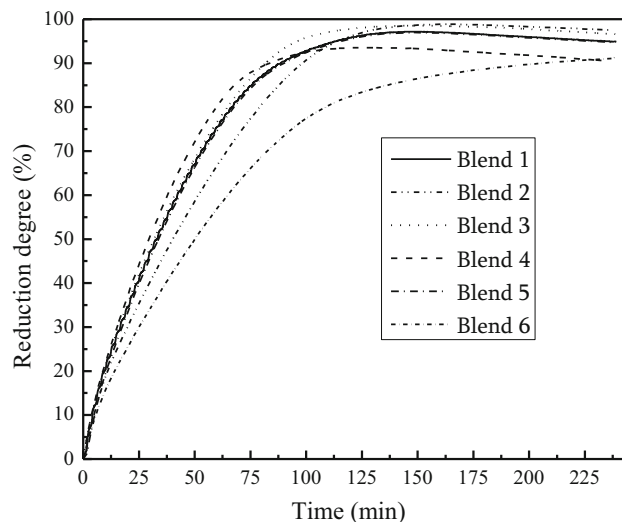


Fig. 11—Effects of ilmenite addition on the reduction of hematite ore sinter.

with ilmenite addition (Figure 12). The porosity was measured using a mercury porosimeter (Quantachrome, PM-22-15).

The reduction behavior of the sinter, especially in the initial stages of reduction, might be related to the total porosity of the sinter, which might be affected by the type of bonding phases formed in the sintering process.^[13] Total porosity was lower in blend 2 than in blend 1, possibly as a result of changes in the morphology of the sinter as a result of the presence of 4CaO·7Fe₂O₃ (s). This type of phase resulted in the sinter with some big platelike columnar morphology (Figure 8(b)), with low gas permeability. The sinter from blend 2 had lower reducibility compared with that from blend 1, particularly during the initial stage of reduction. The sinter from blend 3 had 3CaO·FeO·7Fe₂O₃ (s) and 5CaO·FeAlO₃·4Fe₂O₃·2SiO₂ (s) as the major bonding phases, with some small columnar morphology that showed improved porosity between the columns (Figure 8(c)). This morphology may have improved the gas permeability and reducibility of this sinter in the initial stage of reduction. In contrast, the sinters from blends 4 and 5 had low gas permeability, possibly as a result of the presence of perovskite phase. The presence of the perovskite phase in sinter was reported to affect the fracture toughness of the sinter bonding phases, increasing the generation of cracks.^[1] The presence of cracks in these sinters might have increased their reducibility, especially in the initial stage of the reduction process. Sintered blend 5 (Figure 4(e)) included 2CaO·SiO₂ (s) phase, which is widely known to cause crack propagation during the cooling of sinter due to phase transformation.^[13] Blend 6 sinter had higher total porosity than blend 5 sinter, possibly as a result of the presence of more MgO (s) in blend 6 than in blend 5. However, the presence of CaO·TiO₂·SiO₂ (s), MgO·Fe₂O₃ (s), CaO·FeO·SiO₂ (s), and CaO·Fe_{1.4}Al_{0.6}O₃·SiO₂ (s) might have blocked Fe₂O₃ (s) reduction and decreased the reducibility of blend 6 sinter, even though its porosity increased showing changes in RI, (Figure 13).

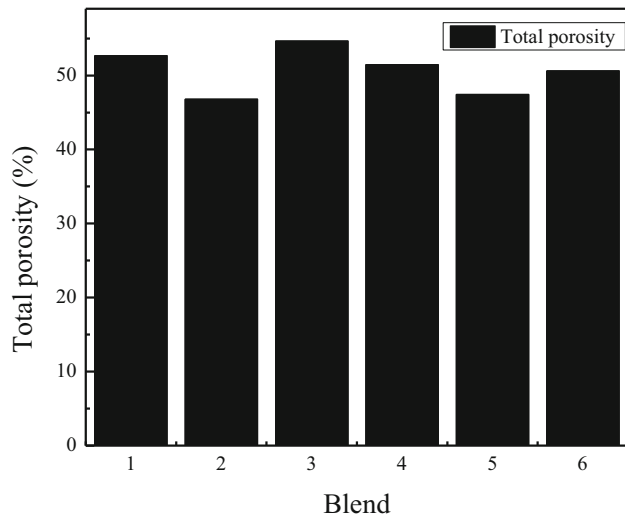


Fig. 12—Effects of ilmenite addition on the total porosity of hematite ore sinter.

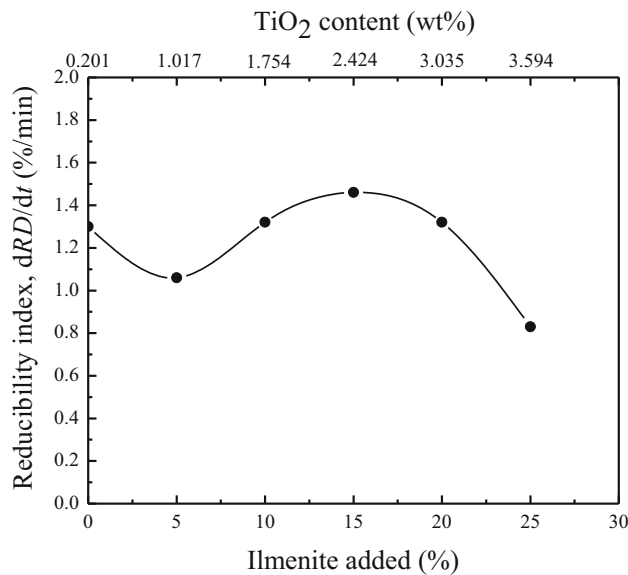


Fig. 13—RI with increasing ilmenite addition.

The reduction degree curves of all the sinters showed slowdown in the rate of reduction at the later stage of the experiment. This change occurs because in the early stages of reduction, the reaction is more likely to be controlled by interfacial chemical reaction, whereas the later stages are likely to be controlled by diffusion.^[23] The reduction reaction in iron ores proceeds by a topochemical receding interface, so the diffusion of the reduction gas is likely to be affected by the morphology of the product in the outer layer of the reduced iron ore pellets. However, additional research on the reaction kinetics of these pellets should be conducted.

RI = dRD/dt varied as the amount of added ilmenite increased. RI initially decreased, possibly as a result of the presence of $4CaO \cdot 7Fe_2O_3$ (s), which has big platelike morphology that may cause low gaseous permeability (Figure 8(b)). Further addition of ilmenite ore increased RI due to formation of $CaO \cdot TiO_2$ (s) within the sintered pellets; this phase increases the occurrence of cracks,^[1] which might increase gas permeability. Sintered blend 4 included $CaO \cdot TiO_2$, $MgO \cdot Fe_2O_3$, and $5CaO \cdot FeAlO_3 \cdot 4Fe_2O_3 \cdot 4Al_2O_3 \cdot 2SiO_2$ phases (Figure 4(d)). The presence of these phases might lead to increased crack propagation during cooling because of the difference in high-temperature thermal-expansion coefficients.^[1] The decreased RI at 25 wt pct ilmenite addition might have been caused by the presence of $MgO \cdot Fe_2O_3$ (s), $CaO \cdot FeO \cdot SiO_2$ (s), and $CaO \cdot Fe_{1.4}Al_{0.6}O_3 \cdot SiO_2$ (s), which might retard the reduction of Fe_2O_3 .

IV. CONCLUSIONS

1. $Ti_{+2\text{ mm}}$ decreased with an increase in the addition of ilmenite up to 20 wt pct. This change might be influenced by the development of bonding phases such as SFCA: The formation of SFCA was affected by the presence of Fe_3O_4 (s) and TiO_2 (s). The availability of TiO_2 (s) in the sinter blends was essential to the formation of $CaO \cdot TiO_2$ (s).
2. Most of the $CaO \cdot TiO_2$ (s) was distributed in the Si-enriched phase, which was believed to be a glass phase.
3. Generation of fines increased with the increase in ilmenite addition. TiO_2 (s) and Fe_3O_4 (s) in the sinter blends are involved in the formation of several different phases as bonding materials that have different high-temperature thermal-expansion coefficients, which might lead to the accelerated crack propagation. The volume expansion caused by reduction of exposed Fe_2O_3 (s) might have promoted crack growth and further deteriorating RDI. An increase in Ti in SFCA with an increase in ilmenite might have affected the strength of the bonding phase that formed.
4. Addition of ilmenite to hematite ore increased the temperature of melt formation in the sinter blends. To clarify the effect of MgO (s) on the hematite-ilmenite ore sinter, the formation mechanism of $CaO \cdot TiO_2$ (s) should be determined.
5. RI = dRD/dt was affected by the phases formed during sintering. The cracks generated by the presence of $CaO \cdot TiO_2$ (s) and calcium silicate increased the gaseous permeability. However, the strength of the sinters made from blends 4 through 6 were so low that they could not be charged into a blast furnace.
6. Addition of < 5 wt pct ilmenite might be recommended for use; at > 5 wt pct, the RDI increases. However, to provide further clarification, additional research should be performed, in which the heating rate, size of sample, and mixing procedure of the raw

material are adjusted to simulate actual industrial conditions.

ACKNOWLEDGMENTS

The authors thank Mr. Wan Ju Kim for help with XRD analysis, Mr. Keun Chang Park for assistance with EPMA operation, and Mr. Lee Sang Ryul for help with gas calibration and preparation of the experimental samples.

REFERENCES

1. N.J. Bristow and C.E. Loo: *ISIJ Int.*, 1992, vol. 32 (7), pp. 819–28.
2. Y.Q. Bai, S.S. Cheng, and Y.M. Bai: *J. Iron Steel Res. Int.*, 2011, vol. 18, pp. 8–15.
3. Z. Wang: *Utilization of Unconventional Ferrous Materials by Sintering*, University of Wollongong, Wollongong, 2015, pp. 1–135.
4. A.D. Manshadi, J. Manuel, S. Hapugoda, and N. Ware: *ISIJ Int.*, 2014, vol. 54 (10), pp. 2189–95.
5. M. Zhou, T. Jiang, S. Yang, and X. Xue: *Int. J. Miner. Process.*, 2015, vol. 22 (9), pp. 917–25.
6. T. Paananen: *The Effects of Minor Oxide Components on Reduction of Iron Ore Agglomerates*, University of Oulu, Oulu, 2013, pp. 1–79.
7. T. Paananen and K. Kinnunen: *Steel ResInt.*, 2009, vol. 80 (6), pp. 408–14.
8. W. Tang, S. Yang, G. Cheng, Z. Gao, H. Tang, and X. Xue: *Minerals*, 2018, vol. 8, pp. 263–77.
9. N.A.S. Webster, J.G. Churchill, F. Tufaile, M.I. Pownceby, J.R. Manuel, and J.A. Kimpton: *ISIJ Int.*, 2016, vol. 56, pp. 1715–22.
10. N.A.S. Webster, M.I. Pownceby, I.C. Madsen, and J.A. Kimpton: *Metall. Mater. Trans. B*, 2012, vol. 43B, pp. 1344–57.
11. L.-H. Hsieh and J.A. Whiteman: *ISIJ Int.*, 1989, vol. 29, pp. 24–32.
12. S. Nicol, J. Chen, M.I. Pownceby, and N.A.S. Webster: *ISIJ Int.*, 2018, vol. 58 (12), pp. 2157–72.
13. A.K. Biswas: *Principles of Blast Furnace Ironmaking*, Cootha Publishing House, Brisbane, 1981, pp. 107–10.
14. S. Jursova, P. Pustejovska, and S. Brozova: *Alex. Eng. J.*, 2018, vol. 57, pp. 1657–64.
15. J.-W. Jeon: *Effects of Magnetite Concentrate on the Assimilation Behavior of Quasi-Particle*, Graduate Institute of Ferrous Technology, Pohang University of Science and Technology, Pohang, 2015, pp. 10–98.
16. S. Dwarapudi, T.K. Ghosh, V. Tathavadkar, M.B. Denys, D. Bhattacharjee, and R. Venugopal: *Int. J. Miner. Process.*, 2012, vols. 112–113, pp. 55–62.
17. D.F. Gonzalez, I.R. Bustinza, J. Mochon, C.G. Gasca, and L.F. Verdeja: *Miner. Process. Extr. Metall. Rev.*, 2017, vol. 38, pp. 254–64.
18. J. Zhang, X. Guo, and X. Huang: *J. Iron Steel Res. Int.*, 2012, vol. 19, pp. 1–6.
19. Q.-J. Gao, G. Wei, Y.-S. Shen, X. Jiang, H.-Y. Zhen, F.-M. Shen, and C.-S. Liu: *J. Cent. South Univ.*, 2017, vol. 24, pp. 2805–12.
20. R. Budzik: *Metallurgija*, 2005, vol. 44, pp. 179–82.
21. G. Zhang and O. Ostrovski: *Int. J. Miner. Process.*, 2002, vol. 64, pp. 201–18.
22. S.K. Gupta, V. Rajakumar, and P. Grieveson: *Metall. Trans. B*, 1991, vol. 22B, pp. 711–16.
23. S. Yang, M. Zhou, X. Xue, T. Jiang, and C. Sun: *JOM*, 2019, vol. 71, pp. 2812–20.

Publisher's Note Springer Nature remains neutral with regard to jurisdictional claims in published maps and institutional affiliations.